SLAC-PUB-1674
November 1975
(T/E)

ANALYSIS OF K^-K^+ AND $\pi^-\pi^+$ FINAL STATES IN 13 GeV K^-p INTERACTIONS*

G. W. Brandenburg†, R. K. Carnegie††, R. J. Cashmore†††, M. Davier‡, T. A. Lasinski, D.W.G.S. Leith, J.A.J. Matthews‡‡, P. Walden‡‡‡, and S. H. Williams

Stanford Linear Accelerator Center
Stanford University, Stanford, California 94306

ABSTRACT

The differential cross sections and density matrix elements for the ϕ and ρ^0 mesons have been measured in the reactions $K^-p \to K^-K^+(\Lambda,\Sigma^0)$ and $K^-p \to \pi^-\pi^+(\Lambda,\Sigma^0)$ at 13 GeV using a wire chamber spectrometer. The analysis shows that while the vector meson production is dominated by the natural parity exchange amplitude, some unnatural parity exchange is also required. Furthermore the ϕ and ρ natural exchange cross sections are identical in shape and have the 2:1 relative strength expected in the quark model with K* and K** exchange degeneracy. The analysis of the clear peak-dip ρ^0-ω interference pattern observed in the $\pi^-\pi^+$ data indicates that the ω production is in phase with the ρ and of similar magnitude. Both the S* and f' meson are clearly observed in this experiment. The S* data are found to be consistent with S* parameters deduced from $\pi\pi$ scattering analyses. The f' density matrix elements and a new limit on the $f' \to \pi^-\pi^+$ branching ratio are presented.

---

*Work supported by the U.S. Energy Research and Development Administration.
†Present address: Dept. of Physics, MIT, Cambridge, Mass.
††Present address: Dept. of Physics, Carleton Univ., Ottawa, Ontario, Canada.
†††Present address: Dept. of Physics, Oxford Univ., Keble Rd., Oxford, England.
‡Present address: Laboratoire de l'Accelerateur Lineaire, Orsay, France.
‡‡Present address: Dept. of Physics, Michigan State Univ., East Lansing, Mich.
‡‡‡Present address: TRIUMF, Univ. of British Columbia, Vancouver, B.C., Canada.

(Submitted to Nucl. Phys. B.)

1.0 Introduction

In this paper we present the results obtained from the analysis of the dipion and dikaon final states produced in the reactions $K^-p \to \pi^-\pi^+ (\Lambda, \Sigma^0)$ and $K^-p \to K^-K^+ (\Lambda, \Sigma^0)$ at 13 GeV. The data come from a high statistics wire spark chamber spectrometer experiment which has been performed at SLAC to study several of the final states in 13 GeV $K^\pm p$ interactions.

The production of dipion and dikaon final states with a K^- beam permits the study of several interrelated topics. The most prominent feature observed in the data is vector meson production. The three vector mesons, the ρ, ω, and ϕ, are produced with comparable hypercharge exchange amplitudes in the K^-p interaction. This is to be contrasted with π induced vector meson production where the ϕ production is very small and where G parity demands different exchanges for ρ and ω production. In this experiment we find that ϕ and ρ production are dominated by the natural parity exchange amplitude, and that the natural parity exchange differential cross sections are identical in shape while differing in magnitude by the expected 2:1 ratio. In addition, the analysis of the striking ρ-ω interference pattern observed in the $\pi^-\pi^+$ data shows that the ω production is in phase with the ρ and similar in magnitude.

Within the context of the quark model, the production of the ϕ-like member of each SU_3 nonet is expected to be enhanced in K^-p interactions. Only the natural spin parity sequence will couple to the $\pi^-\pi^+$ and K^-K^+ final states, and in addition to the ϕ meson, we observe S* and f' production in this experiment.

Vector meson production via hypercharge exchange has been studied at lower energies and included measurements of the polarization of the recoiling Λ or Σ^0 [1, 2, 3]. This experiment extends these measurements to a substantially higher energy, but yields no information on the Λ or Σ^0 polarization since the

recoil baryon is not detected. However, the increased statistics and corresponding sensitivity makes it possible to observe and study other subtle effects such as the ρ-ω interference and S* production for the first time in K^-p interactions.

A brief description of the experimental apparatus and data sample follows in section 2. The production of the ϕ and ρ mesons is analyzed and discussed in section 3. The observation and analysis of ρ-ω interference is presented in section 4. In section 5, the data on S* production in this experiment are compared with the S* parameters deduced from $\pi\pi$ scattering analysis. Finally, the results on f' production including a new limit on the $f' \to \pi^+\pi^-$ branching ratio are presented in section 6.

2.0 The Experiment

2.1 Experimental Apparatus

The experiment was performed in an rf separated 13 GeV K beam at SLAC. Figure 1 shows a plan view of the apparatus [4]. Scintillation counter hodoscopes, two threshold Cerenkov counters, and 1 mm wire spacing proportional chambers were used to measure the mass, momentum, and trajectory of each beam particle incident on the 1-meter-long hydrogen target. The beam resolution is ±0.3% in momentum, ±0.5 mrad in angle, and ±1 mm in space at the interaction point.

The spectrometer system includes 13 magnetostrictive readout wire spark chambers, two on each side of the target, four between the target and the analyzing magnet, and five larger 1.5 m by 3.0 m chambers downstream of the magnet. The dipole magnet aperture is 0.6 m high by 1.8 m wide and the field integral was 18 kg-m. Each of the wire chambers consists of 2 gaps with 4 readout planes and the forward chambers have small polyurethane plugs inserted through which the beam passes. The diameters of the plugs are 3.3 cm upstream and 8.0 cm downstream of the magnet. The spark chamber lever arms are 0.9 m

upstream and 1.9 m downstream of the magnet yielding secondary momentum resolution better than 1%. The observed 13 GeV $K^o \rightarrow \pi^+\pi^-$ decay invariant mass distribution has a FWHM = 12 MeV; the mass distribution for $\phi \rightarrow K^+K^-$ events has a FWHM = 8 MeV. The dimeson production angle is measured to ±1 mrad, while the missing mass squared resolution for identification of the recoil baryon is typically $\sigma = 0.175$ GeV^2.

The trigger for the experiment, defined using several scintillation counter hodoscopes required that 2 or more charged particles pass through the spectrometer after originating from a K^- interaction in the hydrogen target. In addition, the magnet was lined with scintillation counters to reject events in which a secondary particle strikes the pole piece.

The large aperture Cerenkov counter [5] downstream of the spectrometer provided K, π identification of the secondary particles. The counter consists of eight optically distinct mirror-phototube units and was operated with Freon 12 at 1.65 atm. Detailed study of the counter performance indicated that the effective momentum interval for good particle identification was 2.6 to 8.4 GeV for pions and 2.8 to 9.2 GeV for kaons. The choice of pressure and location of the counter was optimized to distinguish the like charge K and π for the study of the $K^-\pi^-\pi^+$ final state and included offsetting the counter to intersect about 85% of the secondaries with the same charge as the incident beam. As a consequence, only a portion (about 35%) of the opposite charge particle trajectories pass through the counter.

2.2 The Data

The large downstream Cerenkov counter is used to identify the K^-K^+ and $\pi^-\pi^+$ final states and thereby to distinguish them from the much more copious reaction $K^-p \rightarrow K^-\pi^+$ (MM). The $\pi^-\pi^+$ events are selected by requiring that the

negative particle be a π^-. This leaves a small contamination from $K^-\pi^+$ events in which the K^- decays, which can easily be corrected for using the measured $K^-\pi^+$ events. In general selection of the K^-K^+ events requires identification of the K^+. However, for the study of the ϕ which is effectively isolated kinematically, the weaker criteria that the positive particle not be labelled a π^+ is used. The contamination from $K^-\pi^+$ events in the ϕ data sample is less than 2%.

The recoil missing mass spectra for events in the ϕ ($1.009 < M(K^-K^+) < 1.029$ GeV) and the ρ^0 ($0.70 < M(\pi^-\pi^+) < 0.84$ GeV) regions are shown in figs. 2a and 2b, respectively. In both distributions, there is a broad peak encompassing both the Λ and Σ^0 hyperons, followed by a substantial dip at 1.3 GeV. Our experimental missing mass resolution is not sufficient to resolve the Λ and Σ^0 peaks, but it provides adequate separation from higher mass hyperon states. There is also a strong peak at the $\Lambda(1520)$ in fig. 2, and some evidence for Y*(1385) production. For the study of the $\phi(\Lambda, \Sigma^0)$ final state, we select events in the interval $1.00 < MM < 1.25$ GeV. For the $\rho^0(\Lambda, \Sigma^0)$ final state, the contaminating $K^-\pi^+n$ events peak at a missing mass of 0.97 GeV; therefore the tighter cut, $1.05 < MM < 1.225$ GeV, is used.

The observed K^-K^+ mass spectrum for $K^-p \rightarrow K^-K^+(\Lambda, \Sigma^0)$ with the K^+ identified is shown in fig. 3a. In addition to a very large ϕ signal (note the change in scale), there is a substantial peak from the f' meson at 1.52 GeV. The histogram has not been corrected for the experimental acceptance, which decreases smoothly with increasing mass. A significant part of the background in fig. 3a arises from $K^-\pi^+$ contamination. Figure 3b shows the K^-K^+ mass distribution in the ϕ region in 2 MeV bins with the less stringent Cerenkov selection criteria discussed above. The reflection of the K*(890) into the K^-K^+ spectrum is peaked near 1.07 GeV and then extends to higher masses. $K^-\pi^+$ feed-through below

1.06 GeV is quite small. The mass cut, $1.009 < M(K^-K^+) < 1.029$ GeV, has been used to select the ϕ data sample, which contains 4808 events.

The $\pi^-\pi^+$ mass spectrum for events recoiling against a (Λ, Σ^0) mass is shown in fig. 4. The sharp peak at the K^0 mass is from $K^-p \rightarrow K^0(n, \Delta^0)$ events for which the missing mass falls within the (Λ, Σ^0) cut. Above the ρ^0 peak, there is evidence for S* production at 0.98 GeV (see section 5) and a broad peaking at the $f^0(1270)$. The histogram is uncorrected for the smoothly varying acceptance. The dashed curve represents the estimated $K^-\pi^+$ contamination; the K*(890) events peak below 0.7 GeV. Actual s wave $\pi^-\pi^+$ background under the ρ^0 does not appear to be very large, the data being consistent with pure p wave in this region (see section 3.1). The $\pi^-\pi^+$ mass cut $0.70 < M(\pi^-\pi^+) < 0.84$ GeV is used to define the ρ^0 data sample, and includes 1410 events.

3.0 ϕ and ρ^0 Meson Production

The production of the ρ^0 and ϕ vector mesons is the most prominent feature observed in the reactions $K^-p \rightarrow \pi^-\pi^+(\Lambda, \Sigma^0)$ and $K^-p \rightarrow K^-K^+(\Lambda, \Sigma^0)$ respectively. These reactions involve hypercharge exchange in the t-channel. In this section we analyze the production and decay distributions of the ρ^0 and ϕ mesons.

3.1 Angular Distribution Analysis

We have extracted the cross sections and the spherical harmonic moments $\langle Y_{\ell m} \rangle$ of both the ϕ and ρ^0 decay angular distributions as functions of $t' = |t - t_{min}|$. The technique used was to perform a maximum likelihood fit of the data to an acceptance corrected sum of spherical harmonics, $Y_{\ell m}$. The corrections for apparatus efficiency, secondary π and K decay, nuclear absorption, and the recoil baryon missing mass cut are incorporated in the Monte Carlo program used to determine the spectrometer acceptance. The average acceptance including all the above factors plus particle identification is 0.50 for the ϕ and 0.15

for the ρ at $t' \sim 0.15$ GeV^2 using the measured angular distributions as input. Fits were done in both the s-channel and the t-channel (Gottfried-Jackson) helicity systems with $\ell, m \leq 2$ assuming that only s and p waves are present in the dimeson system. Since the data showed no evidence for any s wave contribution in either reaction, separate fits with the ℓ=1 moments set to zero corresponding to pure vector meson production were also performed. In the case of the ρ^0 analysis, it was necessary to weight the data on an event by event basis to correct for the $K^-\pi^+$ contamination of the angular distributions.

The s and t channel moments and the corrected differential cross section for $\phi \to K^-K^+$ and $\rho^0 \to \pi^-\pi^+$ are presented in tables 1 and 2 respectively. The moments have been reexpressed in the tables as elements of the spin density matrix, $\rho^{\ell\ell'}_{mm'}$. The p wave elements presented in the tables were obtained from the restricted analysis assuming only p wave production, while the s-p interference elements, Re ρ^{10}_{00} and Re ρ^{10}_{10}, necessarily come from the complete s-p fits.

The density matrix elements Re ρ^{10}_{00} and Re ρ^{10}_{10} are consistent with zero for all t' for both reactions. This means that any s wave background is either incoherent or 90^0 out of phase with the p wave resonances. The latter possibility was ruled out by measuring the values of Re ρ^{10}_{m0} for the upper and lower sides of the resonance peaks; the elements were again found to be zero. In fact any s wave production would be largely incoherent, since an s wave dimeson system must be produced by unnatural parity exchange, while both vector mesons are produced predominantly by natural parity exchange as discussed below. Detailed examination of the K^-K^+ and $\pi^-\pi^+$ mass spectra show no evidence for any s wave under the vector mesons. In section 4 it is demonstrated that a fit to the ρ^0 peak requires no background, although an interfering ω is necessary. This differs from the pion produced ρ^0 where a strong broad s wave enhancement, often called

the ϵ, is observed. Although the coupling of the ϵ to $\bar{K}K$ is below the sensitivity of this experiment, the coupling of the s wave S* through $\bar{K}K \rightarrow S^* \rightarrow \pi^-\pi^+$ is observed and discussed in section 5. The possibility of also observing the S* in the K^-K^+ channel at K^-K^+ threshold does exist, but the observed distribution shown in fig. 3b is entirely accounted for by ϕ resolution and the small $K^-\pi^+$ contamination.

The differential cross sections for $K^-p \rightarrow \phi(\Lambda, \Sigma^0)$ with $\phi \rightarrow K^-K^+$ and for $K^-p \rightarrow \rho^0(\Lambda, \Sigma^0)$ are shown by the solid points in figs. 5 and 6 respectively. These cross sections, and those in tables 1 and 2, have been corrected for the events outside the ϕ and ρ mass cut, and in addition for the ρ a 6% reduction is also made to account for the effects of ρ-ω interference. The ϕ mass cut retains 84% of the ϕ events, while only 60% of the ρ Breit Wigner used in the ρ-ω fit to describe the $\pi^-\pi^+$ mass spectrum is contained within the tight ρ mass cut used here. The estimated systematic error in absolute normalization is ±10% exclusive of the ρ line shape uncertainty.

The ϕ differential cross section shown in fig. 5 has a pronounced forward turnover while beyond $t' = 0.2$ GeV^2, $d\sigma/dt'$ falls off exponentially with a slope of about 3 GeV^{-2}. The ρ^0 differential cross section, although not as well determined, is similar in shape and magnitude to the ϕ cross section. The integrated cross sections for $t' < 1.2$ GeV^2 are 8.0 ± 0.7 μb for $K^-p \rightarrow \rho^0(\Lambda, \Sigma^0)$ and 5.57 ± 0.15 μb for $K^-p \rightarrow \phi(\Lambda, \Sigma^0)$ with $\phi \rightarrow K^-K^+$. Using a $\phi \rightarrow K^-K^+$ branching ratio [6] of 0.466 ± 0.025 gives 12.0 ± 0.5 μb for the total ϕ cross section. The 10% systematic uncertainty in normalization has not been included, and would be common for both the ρ and ϕ result.

3.2 Natural and Unnatural Parity Exchange

To a good approximation at our energy, the density matrix combinations, $\rho_{\pm} = \rho_{11} \pm \rho_{1-1}$, project out the natural (ρ_+) and unnatural (ρ_-) parity exchange components of helicity one vector meson production [7]. The helicity zero state (ρ_{00}) can only be produced by unnatural parity exchange. The differential cross sections for production in each helicity and exchange state, σ_+, σ_-, and σ_0 where $\sigma_i = \rho_i \, d\sigma/dt'$, are shown in figs. 5 and 6 for ϕ and ρ production respectively. σ_+ is invariant under rotations between the s and t channel frames, whereas σ_- and σ_0 are not. It is immediately clear from figs. 5 and 6 that ϕ and ρ^o mesons are produced dominantly by natural parity exchange in the reactions being studied. For the ϕ, σ_+ is approximately 80% of $d\sigma/dt'$ for all values of t'; in the case of the ρ^o the fraction is about 60%.

The dip at t'=0 for σ_+ in figs. 5 and 6 indicates that the dominant contribution to σ_+ is an helicity flip amplitude. The natural parity exchange amplitude must be helicity flip at the meson vertex; if in addition it is nonhelicity flip at the baryon vertex there must be such a dip. On the other hand, if the baryon vertex also has a unit helicity flip, then the total helicity flip can be zero and absorption is expected to decrease the size of the forward dip [8]. To obtain a rough estimate of the fraction of σ_+ which as a net helicity flip of one, we have fit the ϕ data for $t' < 0.5$ GeV^2 to the functional form $c(a+t')\, e^{-bt'}$. The purely exponential term represents the contribution with zero net helicity flip. The values obtained for the parameters were $a = .029 \pm .007$ GeV and $b = 5.9 \pm 0.3$ GeV^{-2}. Integrating the resulting expression over t' we find, for the ϕ, that the fraction of σ_+ with a net helicity flip is $86 \pm 5\%$. We also note that the four ρ^o points for σ_+ are consistent with this fit.

We now turn to the smaller unnatural parity exchange cross sections for the ϕ meson shown in fig. 5. In the t channel, σ_0 for the ϕ has a shape similar to σ_+ but is about 25% in magnitude, while σ_- is small and drops quickly to zero by $t' \sim 0.3$ GeV^2. In the s channel, σ_0 and σ_- are unchanged for small t', but their roles are reversed at large t' with σ_- remaining large. In the s channel, σ_0 has a forward peak and then falls abruptly to zero at $t' \sim 0.4$ GeV^2. The different behavior of σ_0 and σ_- between the two frames can be understood by considering the s-t crossing angle; it is 180° at t'=0, but changes rapidly to 100° by t' = 0.4 GeV, and remains near 90° for larger t'. Thus σ_0 and σ_- are simply interchanged in this region. We note that in both frames the unnatural parity interference element, Re ρ_{10}, is definitely nonzero in the forward direction where both σ_- and σ_0 exist.

The unnatural parity exchange cross sections for ρ° production, shown in fig. 6 in the t channel, differ markedly from those of ϕ production. Because of the effects of the Cerenkov counter tagging requirement on the acceptance, the unnatural parity components of ρ production are not as well determined, especially ρ_{00} in the s channel. However, the unnatural exchange does appear to account for a larger fraction of the cross section and the roles of σ_0 and σ_- in the s and t channel are just the reverse of that for ϕ production. For example in the t channel, σ_- remains a constant fraction (40%) of σ_+ while σ_0 is smaller for most t' values and falls more steeply with t'.

The natural parity trajectories which contribute to the present reactions are K* and K**, while the unnatural parity trajectories are K, Q_A and Q_B. Absorption of the dominant natural parity exchange amplitude could result in some feed-through into the unnatural parity amplitudes. However, in the s channel such feed-through should only affect σ_- and not σ_0 [8]. Furthermore, because σ_+ is

predominantly total net helicity flip, it is not expected to be strongly absorbed. Therefore we conclude that σ_0 and σ_- do indeed represent unnatural parity exchange in the reactions studied. We further note that ρ_+ has risen from ~0.5 at 4 GeV incident energy [1, 2, 3] to ~0.8 at our energy. This rise is consistent with the steeper energy dependence of the unnatural parity exchanges and therefore indicates that both natural and unnatural exchanges are separately present.

3.3 Comparison of ρ and ϕ Production

The cross sections for $K^-p \to \rho^0(\Lambda, \Sigma^0)$, $K^-p \to \omega(\Lambda, \Sigma^0)$ and $K^-p \to \phi(\Lambda, \Sigma^0)$ can be compared using the quark model diagrams shown in fig. 7. Assuming simple t channel exchanges, the ρ^0 and ω cross sections are predicted to be equal in magnitude and phase [1, 9]. The $K^-p \to \phi(\Lambda, \Sigma^0)$ and $K^-p \to \rho^0(\omega)(\Lambda, \Sigma^0)$ cross sections are related by line reversal, assuming the noninteracting top quark line which is different in the two diagrams can be ignored. Additionally, if the t channel amplitudes are exchange degenerate, then the cross section for ϕ production should be twice that for ρ^0 production. The factor of two arises from the fact that the $\bar{p}p$ pair in fig. 7b is an equal mixture of ρ^0 and ω. These predictions also apply to the individual components of the cross section: σ_+, σ_-, and σ_0, and for the Λ and Σ^0 final states independently as well as for their sum.

To compare the experimental data with this prediction, recall that the shape of σ_+ for the ρ^0 was completely consistent with σ_+ for the ϕ (see figs. 5 and 6). Furthermore, the integrated cross sections, σ_+, for $t' < 1.2$ GeV^2 are 5.06 ± 20 μb for the ρ reaction and $4.50 \pm .10$ μb for the ϕ with $\phi \to K^-K^+$. After adjustment for the K^-K^+ branching ratio, σ_+ for the ϕ is $9.7 \pm .4$ μb yielding a ϕ to ρ ratio of 1.91 ± 0.11 in good agreement with the prediction even before the ρ line shape uncertainty is included. This agreement not only suggests that at this energy the K* and K** trajectories are approximately exchange degenerate, but also that

absorption of σ_+ is either weak or equal for ϕ and ρ^0 production. At lower energies, where natural parity exchange is less important, σ_+ for the ϕ is larger than, but not twice, σ_+ for the ρ^0 [1, 2, 3].

It is apparent from figs. 5 and 6 that the prediction is badly broken for the unnatural parity exchange components. In fact, the ϕ to ρ^0 ratio for the total cross section is 1.5 ± 0.2, with the deviation from 2 coming entirely from σ_- and σ_0. The disagreement for unnatural exchange could be the result of exchange degeneracy breaking (for K and Q_B) or absorption.

4.0 ρ^0-ω Interference

4.1 General Remarks

The reaction $K^-p \to \pi^-\pi^+(\Lambda, \Sigma^0)$ should potentially show a strong effect due to ρ^0-ω interference. This follows from the quark model predictions that the ρ^0 and ω production amplitudes should be equal in magnitude and phase [9, 10]. This is in contrast to the effect observed in pion-produced dipion states [11] where the ρ^0 amplitude (dominantly π-exchange) is very much larger than the ω^0 amplitude (ρ and B exchanges). ρ-ω interference has also been seen in ρ^0 photoproduction and with e^+e^- colliding beams, where the ρ^0 and ω amplitudes should be coherent, but where the ω amplitude is smaller by a factor of three [12]. The only previous report of this effect in K^-p reactions was at very low energies where a weak signal was seen [13].

We will assume that ρ^0-ω interference can be described by a coherent sum of normalized Breit-Wigner amplitudes:

$$\sigma(m) = | f_\rho(m) + \alpha e^{i\phi} f_\omega(m) |^2 \qquad (4.1)$$

where the parameters α and ϕ are to be determined from the data. Theoretically, the complex coefficient of f_ω is predicted by the mass matrix formalism [14] to

be

$$\alpha\, e^{i\phi} = \epsilon \frac{A_\omega}{A_\rho} \tag{4.2}$$

where A_ω and A_ρ are vector meson production amplitudes. The variable ϵ, whose modulus squared is just the $\omega \to \pi^+\pi^-$ branching ratio, is given by

$$\epsilon = \frac{\delta}{m_\rho - m_\omega - i\Gamma_\rho/2} \left(\frac{\Gamma_\rho}{\Gamma_\omega}\right)^{1/2} \tag{4.3}$$

and δ measures the electromagnetic mixing of the ρ^o and the ω. The theoretical prediction for the magnitude of δ is 2.5 MeV, and it is expected to be real [15].

Therefore, assuming that δ is real, a measurement of ϕ yields the relative phase of the ρ^o and ω production amplitudes:

$$\begin{aligned} \phi &= \arg\,(A_\omega/A_\rho) + \arg\,(\epsilon) \\ &\simeq \arg\,(A_\omega/A_\rho) + 103^o \quad . \end{aligned} \tag{4.4}$$

The value of α, on the other hand, can be interpreted two different ways. If we assume $\delta = 2.5$ MeV (or alternatively that $|\epsilon|^2$ has been well measured) then α determines the ratio of A_ω to A_ρ:

$$\alpha = |\epsilon| \left|\frac{A_\omega}{A_\rho}\right| \sim 0.13 \left|\frac{A_\omega}{A_\rho}\right| \tag{4.5}$$

If instead we assume the quark model prediction that $A_\omega = A_\rho$ is true, then α^2 can be considered to be a measurement of the $\omega \to \pi^+\pi^-$ branching ratio, $|\epsilon|^2$. It should be noted that the assumption of complete coherence for A_ω and A_ρ means that the measured value of α is essentially a lower limit [13].

4.2 Results

The experimental $\pi^-\pi^+$ mass distribution in the ρ^o region with the $K^-\pi^+$ contamination subtracted is shown in fig. 8. There is a clearly visible distortion

of the ρ^0 peak near the ω mass. The $\pi^-\pi^+$ spectrum peaks quite sharply below the ρ and there is a notch in the spectrum just above the ω mass.

We have fit these data to a coherent sum of acceptance corrected Breit-Wigners plus a possible incoherent linear background. The form of the Breit-Wigner amplitudes used in the fit to expression (4.1) was

$$f(m)\,\frac{m}{\sqrt{q}}\,\frac{m_0\Gamma}{m_0^2-m^2-im_0\Gamma}$$

with

$$\Gamma = \Gamma_0\left(\frac{q}{q_0}\right)^{2\ell+1}\frac{m_0}{m}\,F(q)$$

where m_0, Γ_0 are the nominal masses and widths of the ρ and ω mesons, q is the pion momentum in the dipion rest frame, and we have set the factor $F(q)=1$ for an s wave and $F(q)=\left(1+(Rq_0)^2\right)/\left(1+(Rq)^2\right)$ with $R=1$ fm for a p wave [16].

The fitting function has been smeared by the $\pi^-\pi^+$ mass resolution, which is estimated to be ± 8 MeV. With the ρ^0 and ω parameters fixed at the values [6]

$$m_\rho = 0.765 \text{ GeV} \qquad \Gamma_\rho = 0.150 \text{ GeV}$$

$$m_\omega = 0.7827 \text{ GeV} \qquad \Gamma_\omega = 0.010 \text{ GeV}$$

the best fit to the ρ^0 line shape was obtained with the s wave Breit-Wigner and no additional background. The fit extended from 0.6 to 0.92 GeV and gave a χ^2 of 31 for 29 degrees of freedom (DF); values of the fitted parameters and their statistical errors are $\alpha = 0.19 \pm 0.04$ and $\phi = 99^\circ \pm 10^\circ$.

To test that the interference is a significant effect, we have also performed a fit without the ω contribution. This fit is shown by the dashed curve in fig. 8 and yielded a χ^2 of 81 for 31 DF. The increase of 50 in χ^2 for 2 additional degrees of freedom demonstrates that the interfering ω is indeed required by the data.

We have also used a modified p wave Breit-Wigner [16] for the ρ^o, which does not fit the high mass tail as well ($\chi^2 = 39$ for 29 DF). The results of this fit were $\alpha = 0.21 \pm 0.04$ and $\phi = 104^o \pm 10^o$ showing that the interference parameters are not very sensitive to the ρ^o parametrization. In addition, the ρ mass and width have been varied by ± 10 MeV, the range allowed by previous measurements [6], the ω mass by ± 1 MeV, and the experimental mass resolution by ± 2 MeV. We conclude from these studies that the additional uncertainties due to the parameterization of the fitting function and choice of input parameter values are ± 0.03 for α and $\pm 5^o$ for ϕ. Adding these in quadrature to the statistical errors, our final results are

$$\alpha = 0.19 \pm 0.05$$

$$\phi = 99^o \pm 11^o \quad .$$

Using the assumption discussed in section 4.1 we thus obtain the following relations between the ρ^o and ω production amplitudes:

$$\arg (A_\omega / A_\rho) = -4^o \pm 11^o$$

$$A_\omega / A_\rho = 1.5 \pm 0.4$$

The phase measurement is in excellent agreement with the quark model prediction of amplitudes equal in phase, while the less precise measurement of the ratio is consistent with the prediction.

Alternately if we assume that A_ω and A_ρ are indeed equal, then our measured value of α yields the branching ratio:

$$\frac{\Gamma(\omega \to \pi^+ \pi^-)}{\Gamma(\omega \to \text{all})} = 0.035 \pm 0.018 \quad .$$

This result is larger than, but consistent with the world average [6] of 0.013 ± 0.003. Assuming that the mass mixing parameter α is 2.5 MeV, the theoretically predicted branching ratio is 0.017.

5.0 S* Production

In the $\pi^-\pi^+$ mass spectrum shown in fig. 8 there is a small but distinct peak at 0.98 GeV, which rises above the extrapolated $\rho^0 + \omega$ fit discussed in the previous section (dotted line). We interpret this peak as evidence for the production of the S* meson. Previous evidence for the existence of this state comes from investigations of $\pi\pi$ scattering in π p experiments [17, 18]. In these experiments the $\pi^+\pi^-$ data is observed to drop sharply at $\bar{K}K$ threshold. At the same time there is a threshold enhancement in the K^-K^+ final state. These effects are associated with a drop in the s wave $\pi\pi$ elasticity and indicate the presence of a $\pi\pi$ state, the 0^+ S* meson, which couples strongly to the $\bar{K}K$ channel and is observed through $\pi\pi \rightarrow \bar{K}K$.

In the reaction $K^-p \rightarrow \pi^-\pi^+ (\Lambda, \Sigma^0)$ one can study the inverse process $\bar{K}K \rightarrow \pi\pi$ via K exchange. Since the S* meson is located just at or below K^-K^+ threshold, only this reaction permits direct observation of the entire S* line shape.

The S* peak in our $\pi^-\pi^+$ spectrum contains 35 ± 10 events above background in the mass interval 0.965 - 0.995 GeV. This corresponds to an S* production cross section for this region of 0.20 ± 0.06 μb after correction for spectrometer acceptance, particle identification, and efficiency factors. The effective $S^* \rightarrow \pi^-\pi^+$ acceptance is 0.08. The S* line shape appears to be significantly distorted in this data. The $\pi^-\pi^+$ spectrum rises smoothly to a peak between 0.98 and 0.985 GeV, but then falls very rapidly just above this mass. The data are consistent with no S* contribution above 0.995 GeV. In order to check that the effect we see is in fact due to the S*, we have computed the expected $\pi\pi$ mass dependence from the K matrix parameters determined in previous experiments. The data are replotted in fig. 9 with the ρ^0 tail and the $K^-\pi^+$ contamination

subtracted. The curves in fig. 9 are proportional to

$$q_\pi M_{\pi\pi} |T_{\pi K}|^2 \quad ,$$

where q_π is the pion momentum in the dipion rest system and $T_{\pi K}$ denotes the amplitude for $\bar{K}K \to \pi\pi$ (or $\pi\pi \to \bar{K}K$) †. Each curve was individually normalized to the data in the region $0.94 \leq M_{\pi\pi} \leq 1.02$ GeV; thus the shapes of these curves are predictions from the previous K-matrix fits.

The S* resonance parameters†† which correspond to the K matrix predictions are given in table 3 along with the χ^2 obtained for each fit. Although all three predictions are statistically consistent with the data, the comparisons suggest that the CERN-Munich (Ochs) and the LBL (constant K matrix) curves provide a better description of our data. These solutions are characterized by the presence of only a second sheet pole, whereas the LBL (Case 1) solution has both a second sheet pole and a third sheet "shadow" pole. Unfortunately the S* statistics in this experiment are insufficient to provide a useful constraint on the determination of the S* resonance parameters.

Having observed the S* in the $\pi^-\pi^+$ mass spectrum, it is interesting to check whether an S wave K^-K^+ threshold enhancement exists in the reaction $K^-p \to \bar{K}K^+(\Lambda, \Sigma^0)$. Although the couplings of the S* given in table 3 favor the $\bar{K}K \to \bar{K}K$ channel over $\bar{K}K \to \pi\pi$, the observed K^-K^+ cross section is substantially suppressed by both a factor of q_K/q_π and the fact that most of the S* cross section falls below $\bar{K}K$ threshold. For example, using the CERN-Munich parameters one expects the K^-K^+ cross section below 1.020 GeV to be only 15% of the $S^* \to \pi^-\pi^+$

---

†Our normalization for $T_{\pi K}$ is such that $\sigma(\pi\pi \to K\bar{K}) = 4\pi(q_K/q_\pi)|T_{\pi K}|^2$. The parameters which determine $T_{\pi K}$ are given in refs. [17] and [18].

††The complex couplings are defined as follows. The residues at the pole position E_0 are $R_{ij} = \lim_{E \to E_0} (E_0 - E) T_{ij}$; they satisfy $R_{\pi\pi}R_{KK} - R_{\pi K}^2 = 0$. We may thus take $g_i = +\sqrt{R_{ii}}$ as the dimensionless couplings.

cross section or about 1/2% of the ϕ cross section at 13 GeV. Thus despite the fact the spectrometer acceptance substantially favors the K^-K^+ final state, the few S* events expected can not be isolated in the presence of the very large ϕ signal.

Finally it should be noted that the very small observed S* cross section in the K induced reaction compared to the π induced case is presumably a consequence of the suppression of K exchange relative to π exchange by a factor of the order of $\left(M_\pi^2/M_K^2\right)^2$ at small t.

6.0 The f' Meson

6.1 f' Production

Because the f' production cross sections are small, experimental data on the properties of the f' meson are quite sparse [1, 19]. The K^-K^+ mass spectrum presented in fig. 3a contains a clear peak of 120 events from the f' meson above a smoothly varying background of similar magnitude. Most of the background is due to $K^-p \rightarrow K^-\pi^+X^o$ events in which the π^+ is misidentified in the Cerenkov counter. A fit of a d wave Breit-Wigner plus a linear background to the observed mass spectrum in the mass interval 1.34 to 1.80 GeV gave a good fit ($\chi^2 = 14.3/18$ DF) and the following resonance parameters for the f' meson:

$$M = 1.527 \pm .005 \text{ GeV}$$

$$\Gamma = .061 \pm .008 \text{ GeV}$$

Both results are about 2 standard deviations above the previous average value for the f' parameters [6].

The $f' \rightarrow K^-K^+$ decay angular distribution has been analyzed in order to determine the dominant production mechanism present in $K^-p \rightarrow f'(\Lambda, \Sigma^o)$. In order to perform this analysis, the K^-K^+ angular distribution in the f' region is first corrected for the non f' background using the side band distributions. The f'

angular distribution is then fit with a restricted sum of acceptance corrected spherical harmonic moments. The fit has been performed for a single mass and t' bin, 1.46 - 1.58 GeV and $t' < 1.0$ GeV^2, in both the s and t channel systems. Only the moments Y_{00}, Y_{20}, Y_{22}, Y_{42} were used, motivated by the assumption that only the d wave is present. Good fits of the angular distributions were obtained in both reference frames. However, the s channel fits for the m=0 moments are less reliable because of the restricted acceptance in cos θ due to the particle identification requirements. The results obtained in the t channel expressed as density matrix elements are:

$$\sigma = 2.0 \pm 0.4\ \mu b$$

$$\rho^{22}_{00} = 0.35 \pm .08$$

$$\rho^{22}_{11} = 0.31 \pm .04$$

$$\rho^{22}_{1-1} = 0.20 \pm .05$$

The values of the density matrix elements for f' production found in this analysis are similar to those measured at 4 GeV [1]. In particular, the elements we have neglected were zero within errors in the 4 GeV analysis. When the helicity one density matrix elements are combined to project out f' production by natural and unnatural parity exchange, we find

$$\rho_+ = \rho^{22}_{11} + \rho^{22}_{1-1} = 0.52 \pm .07$$

$$\rho_- = \rho^{22}_{11} + \rho^{22}_{1-1} = 0.11 \pm .05$$

The largest component of f' production, 52%, corresponds to natural parity exchange (K*, K**) as was the case for ϕ production, but the relative strength of the natural exchange compared to the unnatural exchange components has

diminished significantly for the f' relative to the ϕ. This property of the exchange structure for tensor and vector meson production has also been observed for f^o and ρ^o production in $\pi^- p \to \pi^- \pi^+ n$ [20] and is also found to hold for K**(1420) and K*(890) production using the $K\pi$ final state data from this experiment.

6.2 Branching Ratio Limit for $f' \to \pi^- \pi^+$

If the $J^P = 2^+$ nonet is "magically mixed", then the f' meson is a pure $\lambda\bar{\lambda}$ state similar to the ϕ meson. Decay modes to exclusively nonstrange mesons are then expected to be strongly suppressed relative to the dominant $\bar{K}K$ decay (Zweig rule). A new improved upper limit on the $f' \to \pi^- \pi^+$ branching ratio can be obtained in this experiment through the comparison of the dikaon and dipion mass spectra in the f' mass region.

In the $\pi^- \pi^+$ mass spectrum shown in fig. 4, there are 15 events in the mass interval 1.48 to 1.56 GeV. A linear fit to the mass spectrum above the f^o meson indicates that in this interval the background level is 16 ± 2.8 events. Thus we find -1 ± 4.8 $f' \to \pi^- \pi^+$ events, i.e., a null signal. In this same mass interval, 1.48 to 1.56 GeV, there are $N_K = 102 \pm 16$ $f' \to K^- K^+$ events after background subtraction. We use the measured $f' \to K^- K^+$ decay angular distribution as input to the Monte Carlo program to compute the ratio of the spectrometer acceptance for $f' \to K^- K^+$ compared to $f' \to \pi^- \pi^+$, and find an acceptance ratio, $A_{KK}/A_{\pi\pi} = 1.4 \pm 0.1$. If we assume that the rate $f' \to K^o \bar{K}^o$ is the same as the $K^- K^+$ rate, the expected number of $\pi^- \pi^+$ events from $f' \to \pi^- \pi^+$ is

$$N_\pi = 2N_K \frac{A_{\pi\pi}}{A_{KK}} \frac{\Gamma(f' \to \pi^- \pi^+)}{\Gamma(f' \to \bar{K}K)}$$

To compute the branching ratio limit we determine the number of $\pi^- \pi^+$ events required such that a null signal on a 16 ± 2.8 event background corresponds to a

90% confidence level. This gives $N_\pi = 7.3$ events, and yields the result

$$\frac{\Gamma(f' \to \pi^-\pi^+)}{\Gamma(f' \to K\bar{K})} < 0.06 \text{ (90\% CL)}$$

including the uncertainty in the acceptance ratio and $f' \to K^-K^+$ rate.

7.0 Conclusions

We have presented the results of a spectrometer experiment studying the reactions $K^-p \to K^-K^+(\Lambda,\Sigma^0)$ and $K^-p \to \pi^-\pi^+(\Lambda,\Sigma^0)$ at 13 GeV. These reactions yield data on several of the nonstrange mesons. In the dikaon final state, we observe the ϕ and f' mesons. In the $\pi^-\pi^+$ data, the ρ^0, S*, and f^0 mesons are observed while the production of the ω meson is made manifest through the distortion of the ρ^0 line shape from ρ^0-ω interference. No $f' \to \pi^-\pi^+$ signal is seen and a 90% confidence limit of 0.06 on the $\pi^-\pi^+$ decay rate relative to the $f' \to \bar{K}K$ rate is obtained. The f' mass and width parameters measured in this experiment, $M = 1527 \pm 8$ MeV and $\Gamma = 61 \pm 8$ MeV, are both two standard deviations above the previous values for these quantities. The distorted S* line shape observed in this experiment is found to be consistent with the $\pi^-\pi^+$ spectrum predicted using the K matrix parameters determined in previous analyses of $\pi\pi$ scattering near $\bar{K}K$ threshold.

The density matrix elements and cross sections for ϕ, ρ^0, and f' production have been presented. In each case the natural parity exchange amplitude makes the largest contribution to the production cross section. Average values of $\rho_+ = \rho^{\ell\ell'}_{11} + \rho^{\ell\ell'}_{1-1}$ are 0.8 for the ϕ, 0.6 for the ρ, and 0.5 for the f' meson. The data indicate that unnatural parity exchange is also present. Both the ϕ and ρ differential cross sections exhibit forward turnovers. The forward turnover is even stronger for the natural parity exchange part of the cross section, and we find that most of $\sigma_+ = \rho_+ \, d\sigma/dt$ corresponds to an overall helicity flip amplitude

implying helicity nonflip at the baryon vertex. The ϕ and ρ^0 natural exchange differential cross sections are identical in shape and have the relative strength of 2:1 as predicted by the quark model with K* and K** exchange degeneracy. However the t' dependence of the unnatural parity exchange components, σ_0 and σ_-, are very different for the two reactions, and the relative magnitudes are approximately equal indicating either that K and Q_B exchange degeneracy is broken or that absorptive effects are important for the unnatural components.

The $\pi^-\pi^+$ mass spectrum shows a clear peak-dip ρ^0-ω interference pattern. The ρ^0 and ω production amplitudes are found to be in phase and consistent with equality as would be expected from the quark model description of those reactions. The determination of the ρ^0-ω interference parameters is quite stable, and depends only weakly on the Breit-Wigner form used, the ρ^0 or ω mass and width, or the experimental resolution.

We acknowledge the contributions made to this experiment by many other members of our group at SLAC: in particular, A. Kilert, R. Bierce, R. Friday, D. McShurley, and B. Walsh. The contributions of G. Charlton and F. Winkelmann in the early stages of the experiment are appreciated. We also would like to thank the Experimental Facilities, Accelerator Operations, and Computation Center Groups at SLAC for the strong support we received throughout the experiment.

References

1 M. Aguilar-Benitez, S. U. Chung, R. L. Eisner, and N. P. Samios, Phys. Rev. D 6 (1972) 29; R. D. Field, R. L. Eisner, and M. Aguilar Benitz, Phys. Rev. D 6 (1972) 1863.

2 A. Rouge, H. Videau, I. Videau, J. P. DeBrion, L. Moscoso, and R. Radar, Nucl. Phys. B44 (1972) 365.

3 A. J. de Groot, W. Hoogland, B. Jongejans, J. C. Kluyver, G.G.G. Massaro, W. J. Metzger, H.G.J.M. Tiecke, and J.J.M. Timmermans, Nucl. Phys. B74 (1974) 77.

4 G. W. Brandenburg, R. K. Carnegie, R. J. Cashmore, M. Davier, A. Kilert, D.W.G.S. Leith, J.A.J. Matthews, P. Walden, and S. H. Williams, to be submitted to Nucl. Instr. and Methods.

5 H. H. Williams, A. Kilert, and D.W.G.S. Leith, Nucl. Instr. and Methods 105 (1972) 483.

6 Particle Data Group, Phys. Letters 50B (1974) 1.

7 G. A. Ringland and R. L. Thews, Phys. Rev. 170 (1968) 1569; J. P. Ader, M. Cardeville, G. Cohen-Tannoudji, and Ph. Salin, Nuovo Cimento 56A (1968) 952.

8 M. Ross, F. S. Henyey, and G. L. Kane, Nucl. Phys. B23 (1970) 269.

9 H. J. Lipkin, Nucl. Phys. 87 (1968) 321.

10 A. S. Goldhaber, G. C. Fox, and C. Quigg, Phys. Letters 30B (1969) 249.

11 B. N. Ratcliff, F. Bulos, R. K. Carnegie, E. E. Kluge, D.W.G.S. Leith, H. L. Lynch, B. Richter, H. H. Williams, and S. H. Williams, Phys. Letters 38B (1972) 346.

S. L. Kramer, D. S. Ayres, R. Diebold, A. F. Greene, A. J. Pawlicki, and A. B. Wicklund, Phys. Rev. Letters 33 (1974) 505.

P. Estabrooks, B. Hyams, C. Jones, A. D. Martin, P. Weilhammer, W. Blum, H. Dietl, G. Grayer, W. Koch, E. Lorenz, G. Lütjens, W. Männer, J. Meissburger, and U. Stierlin, Nucl. Phys. B81 (1974) 70.

12 R. Marshall, Proc. Int. Conf. on Meson Resonances and Related Magnetic Phenomena, Bologna, 1971, p. 101.

13 S. M. Flatté, Phys. Rev. D 1 (1970) 1.

14 G. Goldhaber, Experimental meson spectroscopy (Columbia University Press, New York, 1970) 59.

15 S. Coleman and S. L. Glaslow, Phys. Rev. 134B (1967) 671.

16 J. Pisut and M. Roos, Nucl. Phys. B6 (1973) 134.

17 B. Hyams, C. Jones, P. Weilhammer, W. Blum, A. Dietl, G. Grayer, W. Koch, E. Lorenz, G. Lütjens, W. Männer, J. Meissburger, W. Ochs, U. Stierlin, and F. Wagner, Nucl. Phys. B64 (1973) 134.

18 S. D. Protopopescu, M. Alston-Garnjost, A. Barbaro-Galtieri, S. M. Flatté, J. H. Friedman, T. A. Lasinski, G. R. Lynch, M. S. Rabin, and F. T. Solmitz, Phys. Rev. D 7 (1973) 1279.

19 I. Videau, H. Videau, A. Rouge, E. Barrelet, J. Badier, J. P. DeBrion, L. Moscoso, J. R. Hubbard, and R. Rader, Phys. Letters 41B (1972) 213.
D. C. Colley, M. Jabes, L. Riddiford, P. M. Watkins, I. Griffiths, C. D. Proter, and R. M. Turnbull, Nucl. Phys. B50 (1972) 1.

20 B. Hyams, C. Jones, P. Weilhammer, W. Blum, H. Dietl, G. Grayer, E. Lorenz, G. Lütjens, W. Männer, J. Meissburger, W. Ochs, and U. Stierlin, Phys. Letter 51B (1974) 272.
A. D. Martin and C. Michael, Nucl. Phys. B84 (1975) 83.

Table 1 (cont'd.)

b) Differential cross section and density matrix elements in s channel.

t' (GeV^2)	$d\sigma/dt'$ ($\mu b/GeV^2$)	ρ^{11}_{00}	ρ^{11}_{11}	ρ^{11}_{1-1}	Re ρ^{11}_{10}	Re ρ^{10}_{00}	Re ρ^{10}_{10}
.00 - .05	7.71 ± .51	.245 ± .049	.378 ± .024	.302 ± .036	-.043 ± .025	.007 ± .032	.001 ± .017
.05 - .10	11.08 ± .54	.200 ± .032	.400 ± .016	.364 ± .021	.043 ± .015	.051 ± .022	.010 ± .010
.10 - .15	12.08 ± .53	.186 ± .028	.407 ± .014	.360 ± .024	.049 ± .014	.014 ± .018	.005 ± .011
.15 - .20	10.92 ± .49	.156 ± .027	.422 ± .014	.349 ± .024	.064 ± .014	.005 ± .019	-.002 ± .011
.20 - .25	9.95 ± .46	.129 ± .027	.435 ± .013	.382 ± .023	.053 ± .013	.009 ± .016	-.014 ± .011
.25 - .30	9.35 ± .44	.031 ± .014	.485 ± .007	.344 ± .029	.039 ± .013	.030 ± .014	.002 ± .013
.30 - .40	6.86 ± .27	.028 ± .015	.486 ± .007	.369 ± .021	.024 ± .011	.000 ± .011	.014 ± .010
.40 - .50	5.13 ± .23	.015 ± .020	.492 ± .010	.323 ± .027	.046 ± .012	-.014 ± .013	.003 ± .013
.50 - .60	3.83 ± .21	-.008 ± .018	.504 ± .009	.308 ± .033	.019 ± .015	-.016 ± .015	.005 ± .016
.60 - .80	2.50 ± .13	-.036 ± .015	.518 ± .008	.375 ± .029	.016 ± .012	-.016 ± .012	-.023 ± .013
.80 - 1.2	1.08 ± .07	.027 ± .032	.486 ± .016	.346 ± .035	.052 ± .018	.010 ± .020	-.005 ± .014

TABLE 1

$K^- p \to K^- K^+ (\Lambda, \Sigma^0)$; $\quad 1.009 < M(K^- K^+) < 1.029$ GeV

a) Differential cross section and density matrix elements in t channel.

t' (GeV^2)	$d\sigma/dt'$ ($\mu b/GeV^2$)	ρ^{11}_{00}	ρ^{11}_{11}	ρ^{11}_{1-1}	Re ρ^{11}_{10}	Re ρ^{10}_{00}	Re ρ^{10}_{10}
.00 - .05	7.69 ± .51	.175 ± .045	.412 ± .023	.268 ± .041	-.076 ± .023	.000 ± .030	.001 ± .019
.05 - .10	11.09 ± .54	.200 ± .032	.400 ± .016	.363 ± .022	-.047 ± .015	.047 ± .021	-.016 ± .012
.10 - .15	12.08 ± .53	.181 ± .029	.409 ± .015	.359 ± .022	-.053 ± .015	.013 ± .019	-.005 ± .010
.15 - .20	10.92 ± .49	.187 ± .030	.406 ± .015	.365 ± .022	-.049 ± .014	.000 ± .019	-.004 ± .011
.20 - .25	9.95 ± .46	.138 ± .025	.431 ± .013	.387 ± .021	-.050 ± .015	-.012 ± .017	-.012 ± .010
.25 - .30	9.35 ± .45	.164 ± .030	.418 ± .015	.411 ± .018	.004 ± .013	.015 ± .019	-.017 ± .009
.30 - .40	6.86 ± .27	.132 ± .023	.434 ± .011	.420 ± .015	.002 ± .010	.018 ± .014	.005 ± .007
.40 - .50	5.13 ± .23	.190 ± .029	.405 ± .014	.411 ± .019	-.016 ± .013	.001 ± .018	.011 ± .009
.50 - .60	3.83 ± .21	.199 ± .034	.401 ± .017	.412 ± .021	.001 ± .016	.004 ± .023	.013 ± .010
.60 - .80	2.50 ± .13	.141 ± .031	.429 ± .015	.464 ± .019	-.009 ± .012	-.033 ± .019	.010 ± .009
.80 - 1.2	1.08 ± .07	.160 ± .043	.420 ± .021	.410 ± .029	.045 ± .016	-.007 ± .020	-.008 ± .014

TABLE 3

Resonance parameters [20] associated with the curves shown in fig. 9

Curve	Pole (MeV)	g_π	g_K	χ^2 (9 bins)
C-M (Ochs) [17]	$(1006 - i15)_{II}$	$0.28 \exp(i76^o)$	$0.55 \exp(-i29^o)$	7.4
LBL (Case 1) [18]	$(997 - i27)_{II}$	$0.30 \exp(-i84^o)$	$0.47 \exp(i11^o)$	16.0
	$(930 - i18)_{III}$	$0.19 \exp(-i65^o)$	$0.63 \exp(i18^o)$	
LBL (Const. K) [18]	$(1002 - i33)_{II}$	$0.35 \exp(-i89^o)$	$0.73 \exp(-i31^o)$	7.0

TABLE 2

$K^- p \to \pi^- \pi^+ (\Lambda, \Sigma^0)$; $0.70 < M(\pi^- \pi^+) < 0.84$ GeV

a) Differential cross section and density matrix elements in t channel.

t' (GeV^2)	$d\sigma/dt'$ ($\mu b/GeV^2$)	ρ^{11}_{00}	ρ^{11}_{11}	ρ^{11}_{1-1}	Re ρ^{11}_{10}	Re ρ^{10}_{00}	Re ρ^{10}_{10}
.00 - .10	16.4 ±2.1	.262±.063	.369±.031	.148±.053	-.059±.047	-.055±.069	.080±.048
.10 - .20	18.0 ±3.2	.142±.043	.429±.022	.168±.115	-.121±.044	-.009±.037	-.035±.037
.20 - .40	12.6 ±1.8	.070±.036	.465±.018	.171±.102	-.092±.033	-.002±.026	-.062±.040
.40 - 1.0	3.06± .73	.066±.067	.467±.033	.271±.210	-.059±.029	.068±.075	.054±.129

b) Differential cross section and density matrix elements in s channel.

.00 - .10	19.9 ±2.9	.447±.095	.277±.047	.136±.029	.085±.026	.021±.058	.028±.010
.10 - .20	16.8 ±3.3	.289±.157	.356±.078	.293±.071	.075±.033	-.002±.082	-.029±.020
.20 - .40	11.3 ±2.0	.209±.149	.395±.075	.315±.071	.074±.035	.073±.067	-.001±.016
.40 - 1.0	3.11± .89	.162±.269	.419±.134	.302±.096	.082±.047	---	---

Figure Captions

1. Plan view of experimental apparatus.
2. Missing mass distributions for (a) $K^-p \rightarrow K^-K^+Y^o$ for $1.009 < m(K^-K^+) < 1.029$ GeV, the ϕ meson region; (b) $K^-p \rightarrow \pi^-\pi^+Y^o$ for $0.70 < m(\pi^-\pi^+) < 0.84$ GeV, the ρ^o meson region.
3. Observed K^-K^+ mass distribution for $K^-p \rightarrow K^-K^+ (\Lambda, \Sigma^o)$. (a) Cerenkov identification of the K^+ required. (b) The ϕ meson region with the Cerenkov counter selection only requiring the positive particle not be labelled a π^+.
4. Observed $\pi^-\pi^+$ mass distribution for $K^-p \rightarrow \pi^-\pi^+ (\Lambda, \Sigma^o)$. The dashed curve gives the estimated background from misidentified $K^-p \rightarrow K^-\pi^+X^o$ events.
5. Differential cross section for $K^-p \rightarrow \phi (\Lambda, \Sigma^o)$ with $\phi \rightarrow K^-K^+$. The cross section, $\sigma_0 = \rho_{00}\, d\sigma/dt'$, gives the helicity zero component produced by unnatural parity exchange. $\sigma_\pm = (\rho_{11} \pm \rho_{1-1})\, d\sigma/dt'$ describe the natural (σ_+) and unnatural (σ_-) parity exchange helicity one component. σ_0 and σ_- are presented for both (a) the t channel and (b) the s channel helicity frames.
6. Differential cross section for $K^-p \rightarrow \rho^o (\Lambda, \Sigma^o)$. $\sigma_0 = \rho_{00}\, d\sigma/dt'$ gives the unnatural exchange helicity zero component. $\sigma_\pm = (\rho_{11} \pm \rho_{1-1})\, d\sigma/dt'$ describe the natural (σ_+) and unnatural (σ_-) parity exchange helicity one component. σ_0 and σ_- are presented in the t channel.
7. Quark model reaction diagrams for (a) $K^-p \rightarrow \phi\Lambda$ and (b) $K^-p \rightarrow \rho^o\Lambda$ or $K^-p \rightarrow \omega\Lambda$.
8. Observed $\pi^-\pi^+$ mass distribution with the background events from $K^-p \rightarrow K^-\pi^+X^o$ subtracted. The solid curve is the result of a fit to these data of a coherent sum of acceptance corrected ρ^o and ω Breit-Wigner amplitudes ($\chi^2 = 31/29$ DF). The dashed curve gives the best fit when only the ρ amplitude is present ($\chi^2 = 81/31$ DF). The dotted line is the extrapolation of the ρ^o-ω fit above 0.92 GeV^2.

9. Observed $\pi^-\pi^+$ mass distribution in the S* meson mass region with both the $K^-p \rightarrow K^-\pi^+X^o$ background and $K^-p \rightarrow (\rho^o, \omega)(\Lambda, \Sigma^o)$ events subtracted. The curves are the predicted S* line shape normalized to this data obtained from three different solutions for the S* parameters given by previous $\pi\pi$ scattering analyses (see text).

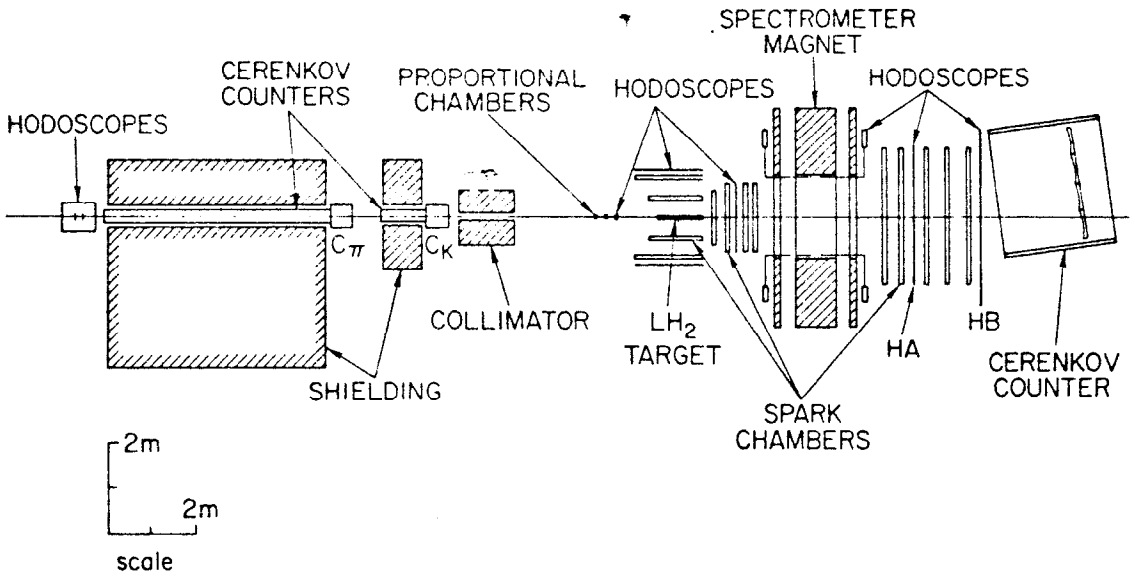
SPECTROMETER MAGNET
CERENKOV COUNTERS
PROPORTIONAL CHAMBERS
HODOSCOPES
HODOSCOPES
HODOSCOPES
C_π
C_K
COLLIMATOR
LH_2 TARGET
HA
HB
CERENKOV COUNTER
SHIELDING
SPARK CHAMBERS
2m
2m
scale

Fig. 1

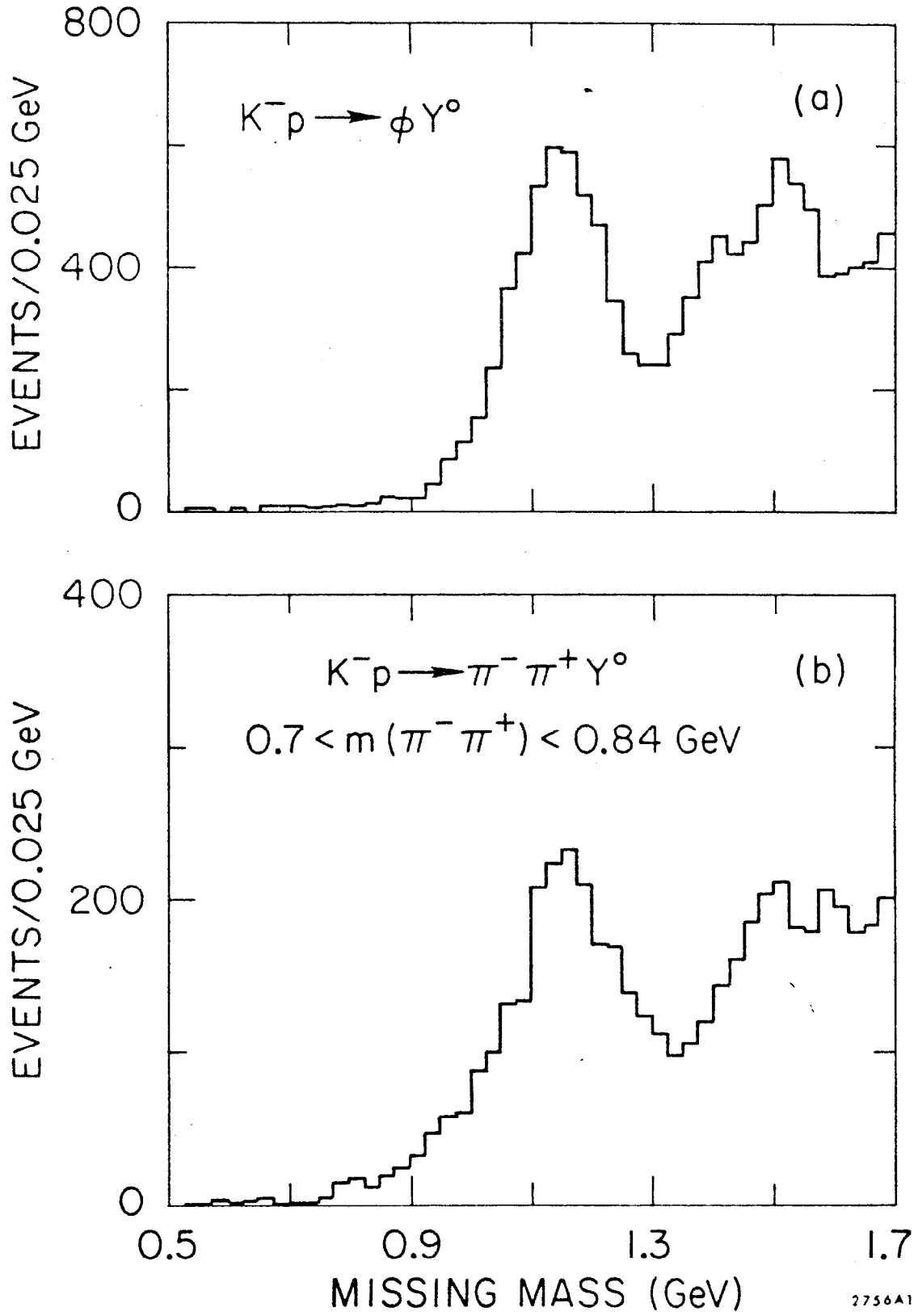
800
400
0
EVENTS/0.025 GeV
$K^-p \rightarrow \phi Y^\circ$
(a)
400
200
0
EVENTS/0.025 GeV
$K^-p \rightarrow \pi^-\pi^+ Y^\circ$
(b)
$0.7 < m(\pi^-\pi^+) < 0.84$ GeV
0.5
0.9
1.3
1.7
MISSING MASS (GeV)
2756A1

Fig. 2

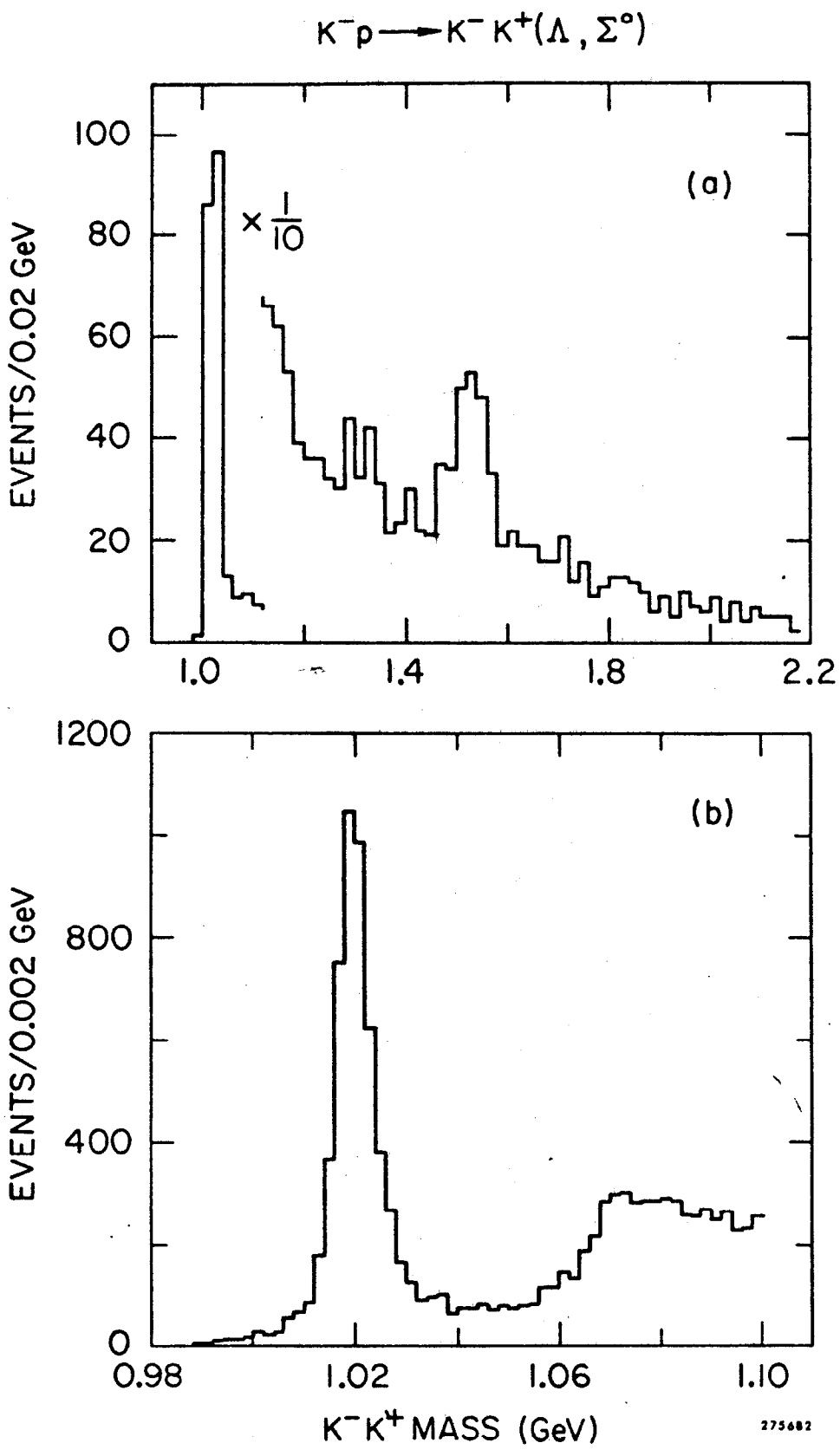
$K^-p \longrightarrow K^- K^+(\Lambda, \Sigma^\circ)$
(a)
$\times \frac{1}{10}$
EVENTS/0.02 GeV
100
80
60
40
20
0
1.0
1.4
1.8
2.2
(b)
EVENTS/0.002 GeV
1200
800
400
0
0.98
1.02
1.06
1.10
$K^- K^+$ MASS (GeV)
275682

Fig. 3

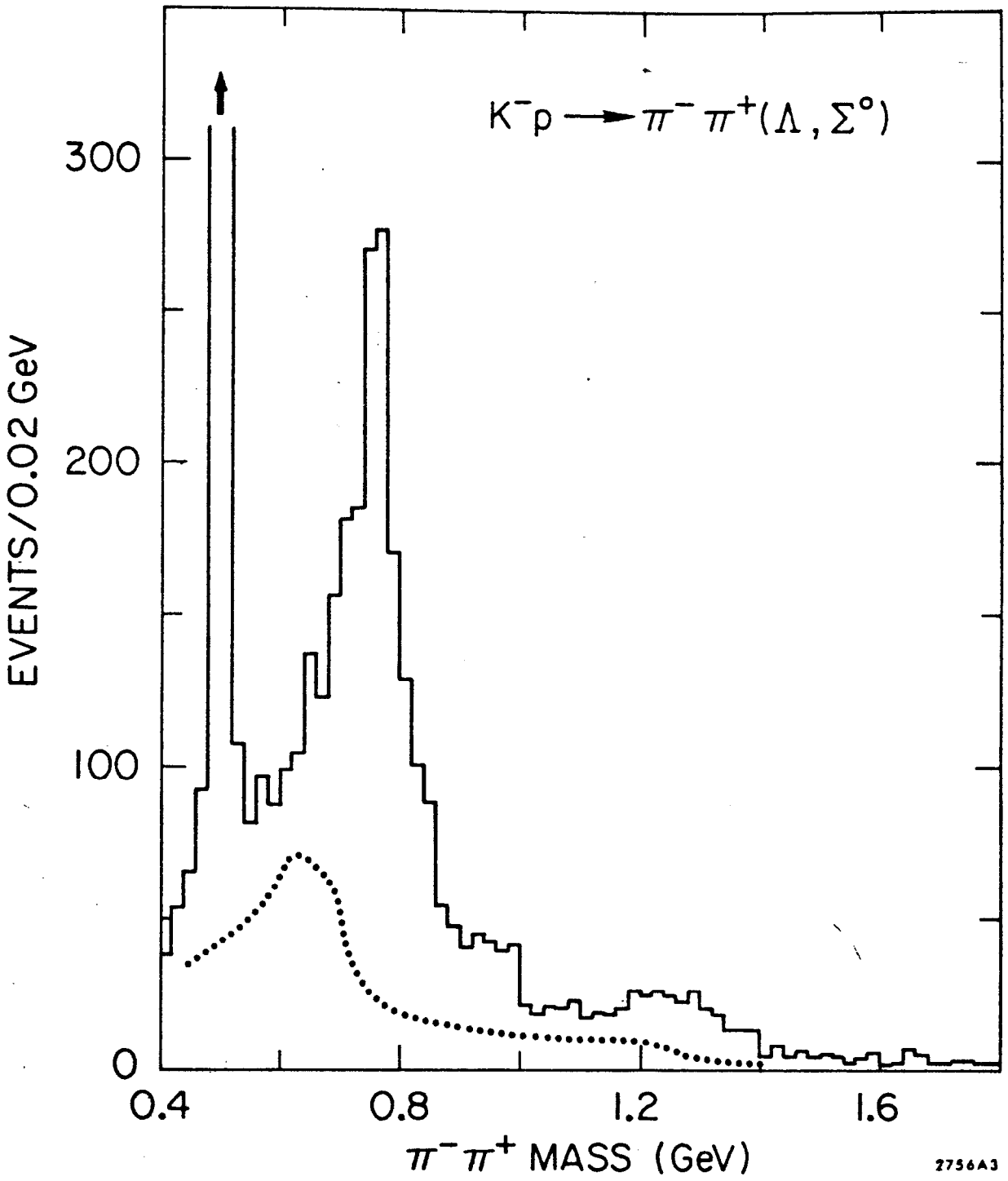
$K^- p \rightarrow \pi^- \pi^+ (\Lambda, \Sigma^\circ)$
300
200
100
0
EVENTS/0.02 GeV
0.4
0.8
1.2
1.6
$\pi^- \pi^+$ MASS (GeV)
2756A3

Fig. 4

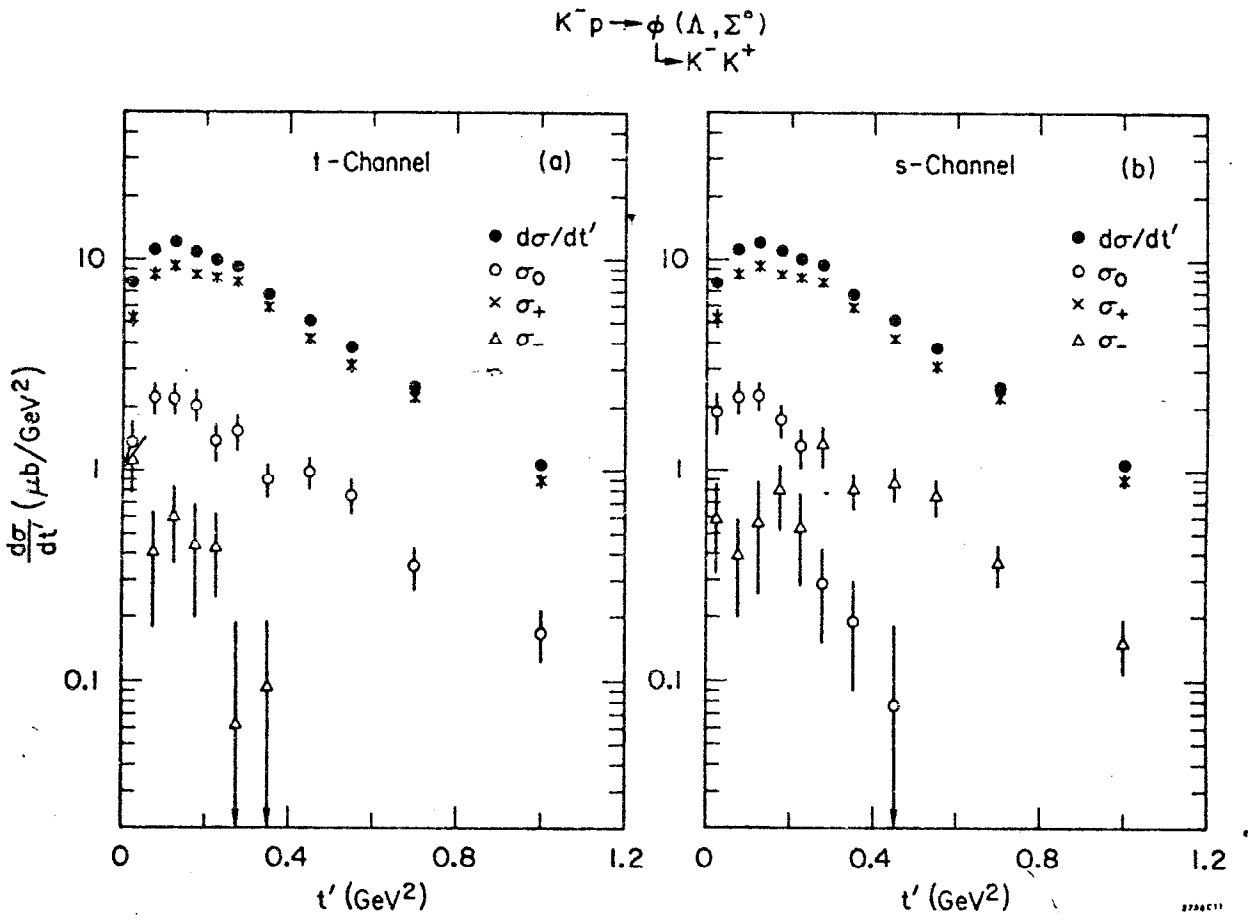
K⁻p → φ (Λ, Σ°)
└→K⁻K⁺
t-Channel
(a)
s-Channel
(b)
dσ/dt'
σ0
σ+
σ−
10
1
0.1
0
0.4
0.8
1.2
t' (GeV²)
dσ/dt (μb/GeV²)

Fig. 5

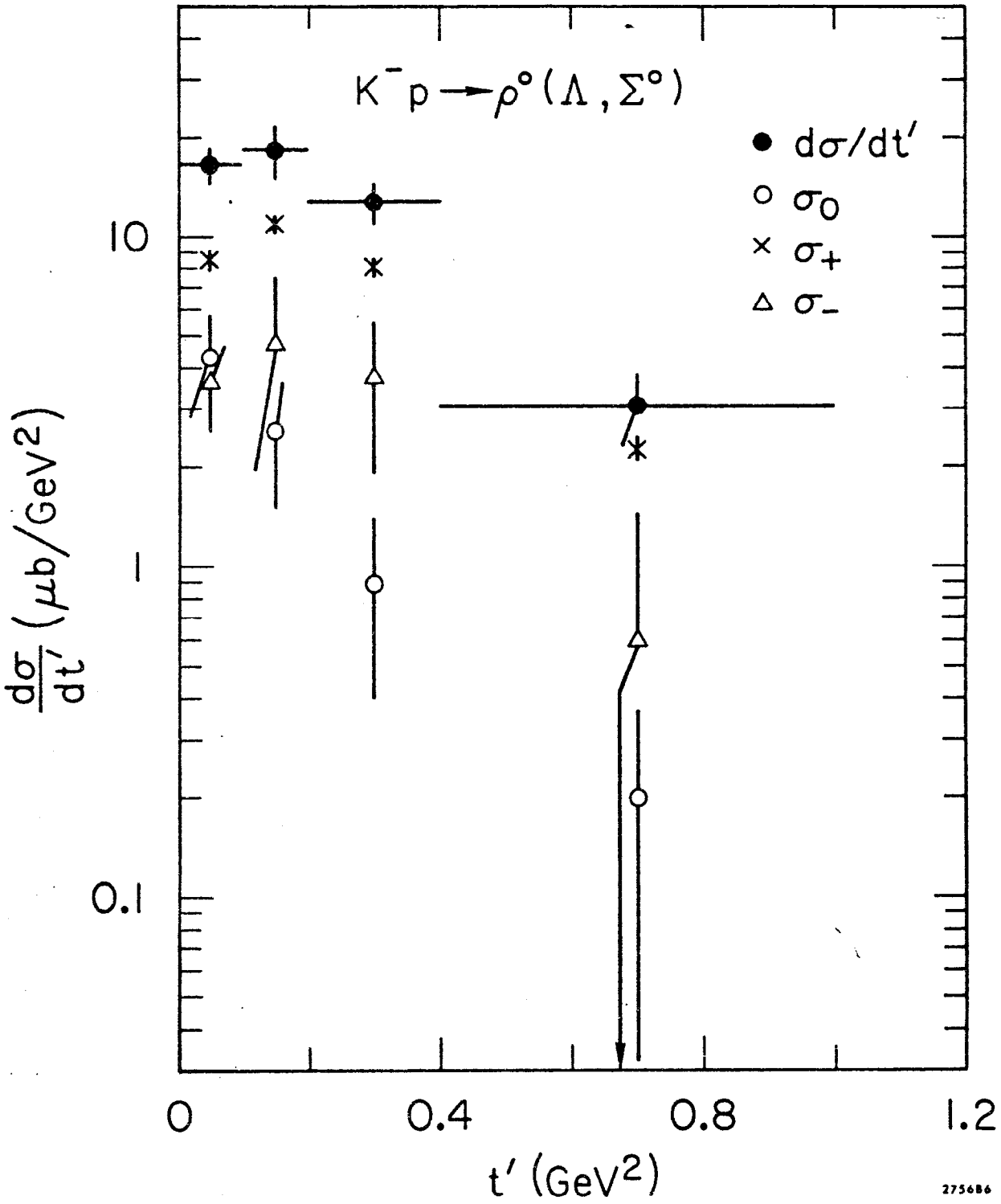
$K^- p \rightarrow \rho^0 (\Lambda, \Sigma^0)$
$d\sigma/dt'$
σ_0
σ_+
σ_-
10
1
0.1
$\frac{d\sigma}{dt'}$ (μb/GeV^2)
0
0.4
0.8
1.2
t' (GeV^2)
275686

Fig. 6

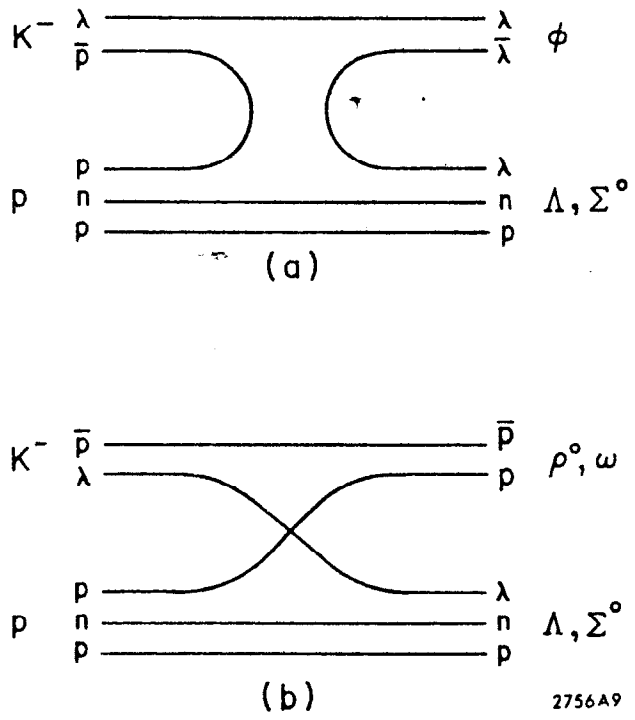

Fig. 7

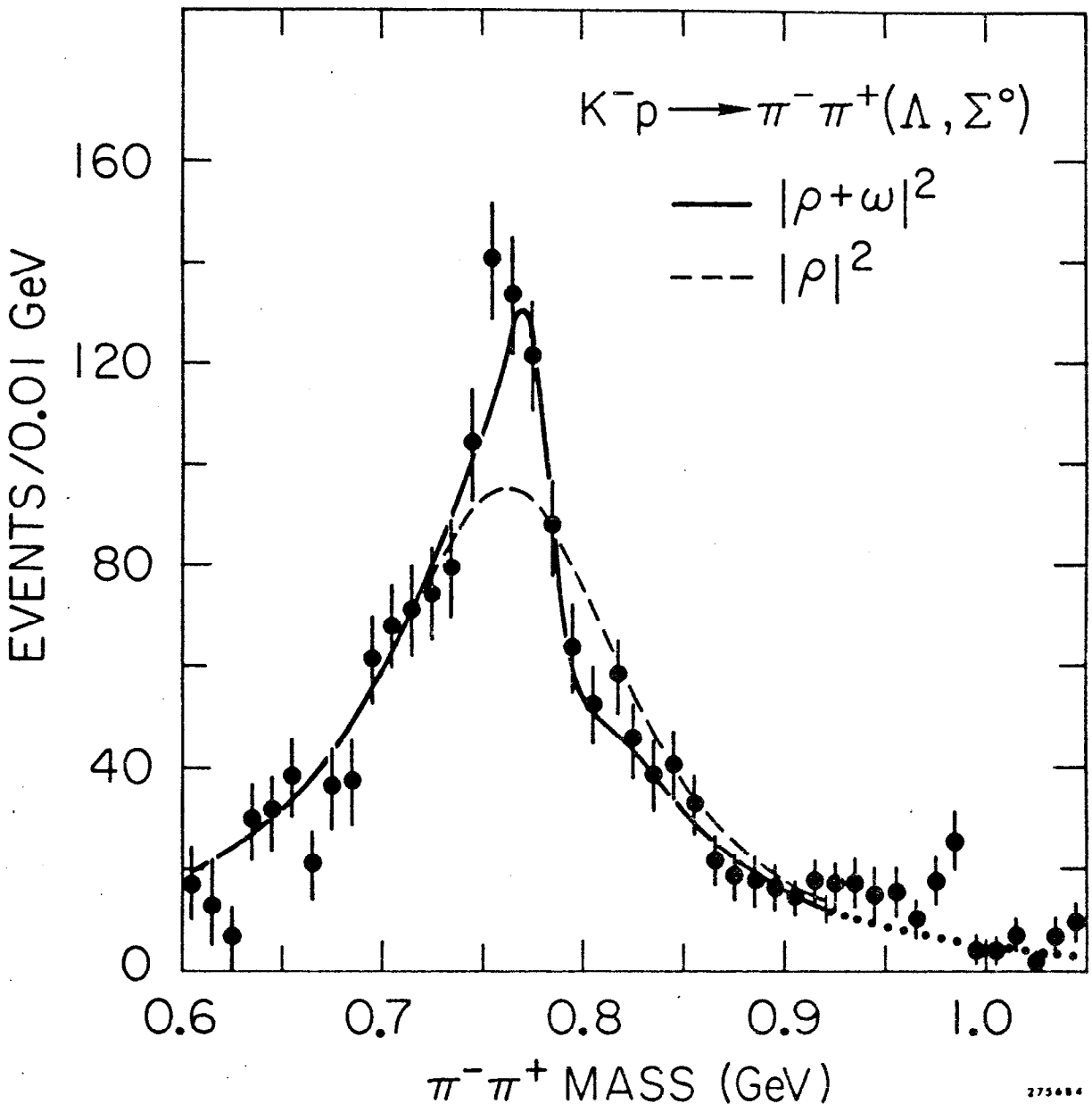
$K^-p \rightarrow \pi^-\pi^+(\Lambda, \Sigma^\circ)$
$|\rho+\omega|^2$
$|\rho|^2$
EVENTS/0.01 GeV
160
120
80
40
0
0.6
0.7
0.8
0.9
1.0
$\pi^-\pi^+$ MASS (GeV)

Fig. 8

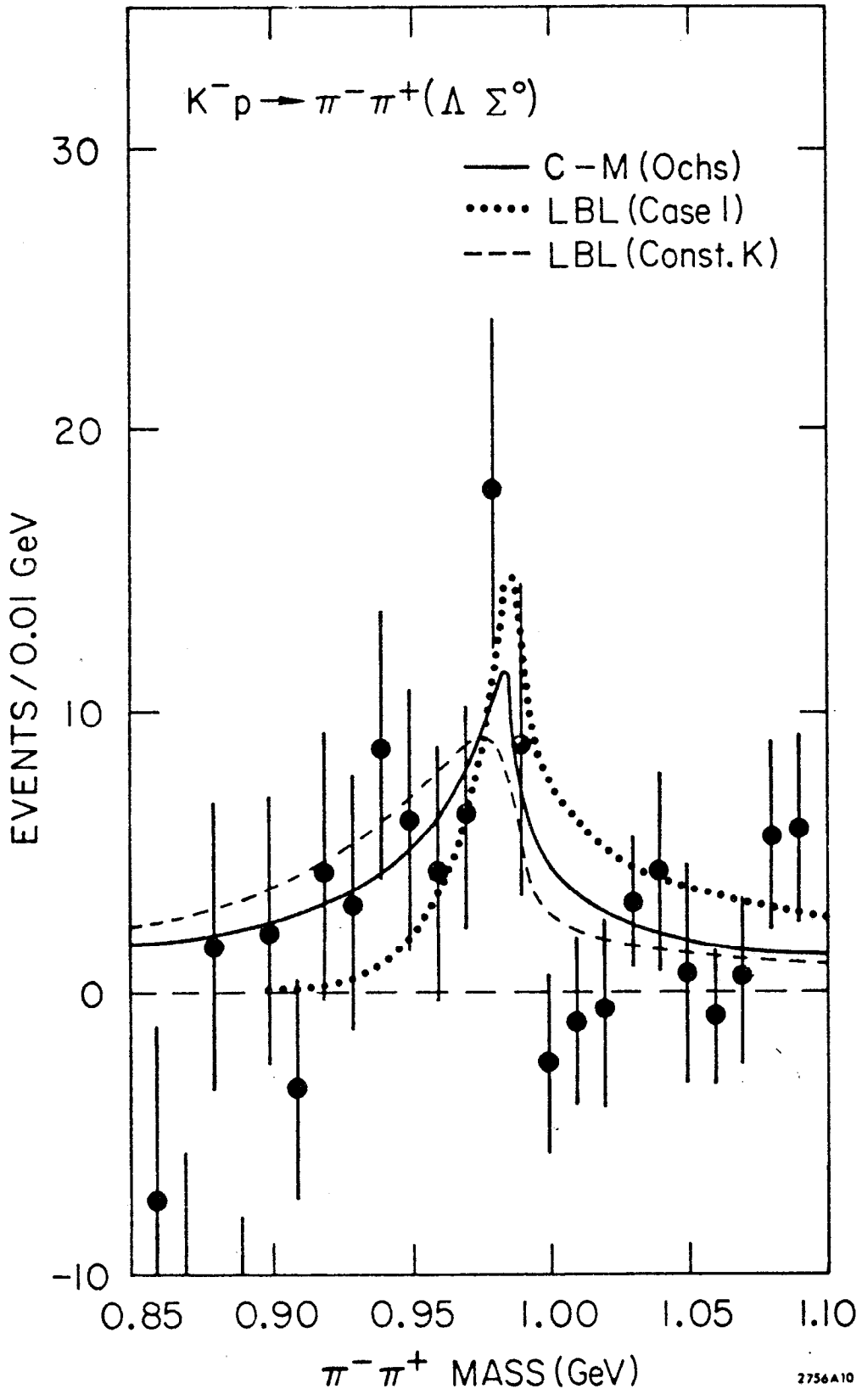
$K^- p \rightarrow \pi^- \pi^+ (\Lambda\ \Sigma^\circ)$
C – M (Ochs)
LBL (Case I)
LBL (Const. K)
EVENTS / 0.01 GeV
30
20
10
0
-10
0.85
0.90
0.95
1.00
1.05
1.10
$\pi^- \pi^+$ MASS (GeV)
2756A10

Fig. 9